Magnetic Resonance Imaging for Improved Brain Tumor Detection

Blake Benyard[1], Narayan Datt Soni[1], Anshuman Swain[1], Nishi Srivastava[2], Sunil Kumar Khokar[1], Nadir Yehya[2], Yi Fan[3], Dushyant Kumar[1], Ravi Prakash Reddy Nanga[1], Michael P. Frenneaux[4], Mohammed Haris[1], Ravinder Reddy[1]

[1]Center for Metabolic Imaging in Precision Medicine (CAMIPM), Department of Radiology, Perelman School of Medicine at the University of Pennsylvania, Philadelphia, Pennsylvania, USA

[2]Department of Anesthesiology and Critical Care Medicine, Children's Hospital of Pennsylvania, Philadelphia, PA, USA

[3]Department of Radiation Oncology, University of Pennsylvania, Philadelphia, PA, USA

[4]Hamad Medical Corporation, Doha, Qatar

**Blake Benyard and Narayan Datt Soni contributed equally to this work.

Abstract

Precise demarcation of brain tumor boundaries is critical for optimizing treatment strategies and improving patient outcomes. *In vivo* characterization of tumor using PET/CT and MRI is clinical standard. PET/CT highlights the metabolic aspects of the tumor, while MRI provides information on functional, metabolic and structural changes. Even with technological advancements in both PET/CT and MRI, a method that can precisely delineate infiltrative tumor boundaries from normal-appearing brain regions (NABR) *in vivo* is still lacking. To address this limitation, we explored a relatively new MR imaging method, the Nuclear Overhauser Effect Magnetization Transfer Ratio (NOE_{MTR}), in conjunction with a gadolinium-based contrast agent (Gd-DOTA), to precisely delineate the tumor boundaries in a rat model of infiltrative gliosarcoma. NOE_{MTR} imaging was performed in the rat model (n=5) before and after Gd-DOTA administration. The post-Gd-DOTA NOE_{MTR} map was subtracted from the pre-Gd-DOTA map and compared with contrast-enhanced T_1-weighted images and immuno-histological findings. The resulting NOE_{MTR} difference map clearly highlighted both the tumor core and infiltrative boundaries, which was not discernible on the post-contrast T_1-weighted images. The extended tumor boundaries observed on the NOE_{MTR} difference map corroborated with the IHC image, which confirmed the presence of infiltrative tumor cells and macrophages in these regions. Guided by the NOE_{MTR} difference map, regions of interest (ROI) were drawn to quantify NOE_{MTR} signal changes in the tumor core, tumor boundaries, and NABR post-Gd-DOTA. Tumor core showed a significant ~43% reduction in NOE_{MTR} signal ($p = 0.003$), while the tumor periphery exhibited a moderate reduction of ~10%, ($p = 0.045$). No appreciable change in was observed in the NABR ($p = 0.371$). In contrast, the post contrast T_1-weighted signal changes in tumor core, tumor periphery and NABR were, 33.32% ($p = 0.092$), 3.8% ($p = 0.478$), and 8.7% ($p = 0.464$) respectively. These findings suggest that NOE_{MTR} imaging provides enhanced tumor contrast, particularly at the infiltrative tumor margins, where conventional contrast enhanced T_1-weighted MRI may underestimate tumor extent. Histological validation confirmed the presence of infiltrative tumor cells and macrophages in the tumor periphery, as highlighted by the NOE_{MTR} difference map. Overall, NOE_{MTR} imaging, in combination with Gd-DOTA administration, demonstrates superior delineation of brain tumor boundaries compared to conventional MRI. As NOE_{MTR} imaging is a fast acquisition scan (under 10 minutes) and performed on standard 3 Tesla, it can be easily integrated into clinical protocols. By improving visualization of tumor infiltration and distinguishing tumor regions from NABR, NOE_{MTR} imaging holds promise for advancing neuro-oncological diagnostics and treatment planning.

Introduction

Accurate tumor identification and precise delineation of brain tumor boundaries are essential for clinicians to tailor interventions, optimizing treatment strategies, guide surgical resection while minimizing damage to surrounding healthy tissue, and assess patient prognosis[1, 2-6]. A multicenter cohort study found that maximal resection of the contrast-enhanced (CE) tumor is associated with improved overall survival in all patients with newly diagnosed glioblastoma, regardless of age, IDH mutation status, or MGMT (O6-methylguanine-DNA methyltransferase) methylation[7]. Importantly, in patients younger than 65 years, aggressive resection of both CE and surrounding non-contrast-enhanced (NCE) tumor regions significantly improved overall survival, regardless of tumor subtype[7]. Another recent study showed that supramaximal resection of NCE tumor regions improved overall survival for all newly diagnosed patients with IDH wild-type glioblastoma[8]. These findings support a revised surgical approach in which maximal NCE tumor resection is prioritized for GBM patients, regardless of molecular subtype. This underscores the clear need for precise demarcation of tumor boundaries to enable safe resection while avoiding damage to normal brain regions, which cannot be achieved through random surgical removal of NCE regions.

Although Computed Tomography (CT) and Positron Emission Tomography (PET) using ^{18}F-FDG are widely used for tumor diagnosis, they are unable to accurately delineate tumor peripheries. Moreover, their reliance on ionizing radiation limits their repeated use for monitoring therapeutic efficacy. In contrast, conventional Magnetic Resonance Imaging (MRI) does not involve radiation and can be safely used multiple times without adverse effects, making it more suitable for ongoing assessment and treatment planning. However, conventional magnetic resonance imaging (MRI) techniques often face challenges in distinguishing tumor margins due to the complex and heterogeneous nature of brain tumors[9-12]. In particular, the transition between tumor tissue and normal-appearing brain regions (NABR) can be subtle, lacking well-defined edges, which complicates treatment planning[13].

Till date contrast-enhanced T_1-weighted MRI remains the gold standard for visualizing brain tumors and differentiating them from NABR[14]. This technique relies on the accumulation of contrast agents such as gadolinium-based compounds in the extracellular-extravascular space (EES) of tumor tissue, providing enhanced visibility of abnormal regions. Despite its widespread use, several limitations persist, including insufficient contrast between tumor and peritumoral regions, partial volume effects that obscure finer structural details, and difficulties in detecting tumor infiltration into the surrounding brain tissue[14]. These challenges are particularly pronounced in infiltrative tumors, where malignant cells may extend beyond the visibly

enhanced regions, leading to potential underestimation of tumor extent and suboptimal treatment planning.

To address these limitations, Nuclear Overhauser Effect (NOE)-weighted MRI has emerged as a promising alternative, offering enhanced sensitivity to molecular and structural changes in the tumor microenvironment[16-29]. This advanced imaging technique leverages indirect detection of membrane lipids and other macromolecular interactions, providing contrast based on biophysical properties rather than solely depend on gadolinium uptake. Given that tumor cells often exhibit compromised plasma membrane integrity, NOE-mediated magnetization transfer ratio (NOE_{MTR}) imaging has the potential to improve discrimination between tumor tissue and NABR[29].

In this study, we explored the potential of NOE_{MTR} imaging in combination with gadoterate meglumine (Gd-DOTA) administration to enhance tumor contrast and improve visualization of tumor boundaries. By integrating NOE_{MTR} with conventional contrast-enhanced MRI, we aim to capture a more comprehensive representation of tumor extent, potentially overcoming the limitations of standard imaging methods. This study investigates the advantages of NOE_{MTR} imaging in providing a more precise delineation of brain tumors, thereby improving diagnostic accuracy and effective therapeutic strategies.

Methods

The experimental protocols used in this study were approved by the Institutional Animal Care and Use Committees of the University of Pennsylvania. Five Sprague-Dawley rats (~6 weeks old), weighing ~140 g, were used to generate tumor-bearing rat model. Briefly, rats were anaesthetized using isoflurane and hair on their scalps were removed using a hair trimmer and hair removal cream. Rats were positioned with head fixed on the stereotaxic apparatus equipped for a continuous supply of isoflurane to induce a surgical plane of anesthesia. Bupivacaine (under the scalp; 2mg/kg) and meloxicam (subcutaneous; 2mg/kg) analgesics were administered. After sterilizing the scalp an incision was made to expose the skull. Following stereotaxic navigation to 3mm lateral (right) and 3mm posterior to bregma a burr hole was drilled to inject a 5µl suspension containing ~50,000 gliosarcoma (F98) cells in phosphate buffer into the cerebral cortex (2mm deep) using a Hamilton syringe and a 32-gauge needle.

Following two weeks post tumor implantation, MRI was performed on isoflurane (1.5%) anaesthetized rats using a 9.4T horizontal bore preclinical MR scanner (Bruker) and a 30-mm diameter proton volume coil (m2m Imaging Corp., OH). Breathing (60/minutes) and temperature (37°C) were maintained throughout the scan.

A localizer was acquired first, followed by a T1-weighted FLASH (TE=□4 ms , TR = 498□ms, four averages, 16 slices) and T2-weighted RARE (TE1/TE2□=□33/121□ms, TR□=□3s, two averages, 16 slices, rare factor□=□6. For NOE MRI acquisitions, a water saturation shift referencing (WASSR) image (TE =□4 ms, TR= 410□ms, 22 frequency offsets from 0 to 1□ppm in steps of 0.1ppm, B_{1rms} □=□0.1μT) was acquired for correcting B_0 inhomogeneities (Kim et al., 2009). A full Z-spectrum was acquired for the saturated images with 52 offsets from +5 to -5 ppm in steps of 0.2 ppm).The acquisition parameters included: TE=□4, TR = 3s, B_1□=□1.0 μT, saturation duration (tsat)□=□3s, and two averages. An unsaturated image (with the same parameters as the saturated images, was additionally acquired. The FOV was 20□mm x 20□mm with an image matrix size of 128 × 128, resulting in an in-plane resolution of 0.156□mm x 0.156□mm for all images.

An intravenous injection (IV) of a gadolinium-based contrast agent (Gadoterate meglumine, Dotarem, France; 0.1mmol/kg) (Gd-DOTA) was administered through a pre-inserted catheter in the tail vein. To monitor changes in the signal intensity T_1-weighted images and canonical Z spectrum data were acquired again on the same slice 30 minutes post injection. After imaging, the rats were perfused, and the brains were extracted for hematoxylin staining. A timeline description of the methodology is shown in Figure 1.

All image processing steps were performed on MATLAB 2022a (MathWorks, CA) and NOE_{MTR} was calculated using following expression to generate contrast maps:

$$\boldsymbol{NOE_{MTR}}\ (\%) = \mathbf{100} * \frac{S_0 - S(-3.5\ ppm)}{S_0},$$

where S_0 is the signal intensity without saturation or saturation pulse applied at 100 ppm (NONE). To delineate the tumor boundary, post Gd-DOTA NOE map was subtracted from the pre Gd-DOTA NOE map.

Immunohistochemistry: After dissection and fixation for 24 hrs in 4% cold paraformaldehyde, rat brains were washed in 1X PBS and processed through a series of alcohols, xylenes and wax for 14 hours followed by embedding in paraffin. Thin 5 µm paraffin coronal sections of brain were collected from the tumor site and mounted onto the slides. After drying overnight, slides were baked at 60°C for 20 min, followed by rehydration through xylenes and graded alcohols, and water. For antigen retrieval, slides were then exposed to a 60°C wash with 1X citrate buffer (#H-3300; Vector labs) for 30 min, and, following rinses in PBS, they were incubated at 37°C in 20µg/ml Proteinase K/1xPBS, and treated with a 15 min wash in 3% H_2O_2 to block endogenous peroxidase.

Slides were placed in humid chamber with 3% bovine serum albumin (1X PBS), for 1 hr at room temperature. Each section was treated with a 1:500 dilution of Mouse-anti-rat ED1 (CD68) (BioRad # MCA341GA) overnight at 4°C in humid chamber. After washing in 1X PBS, sections were treated with horse-anti-mouse biotinylated antibodies from Vector labs (Newark, CA) for 30 min through their peroxidase ABC kit (PK-6200) according to manufacturer's instructions. After washing in 1X PBS the sections were treated with chromogenic immPACT DAB (Vector labs; SK-4100). This was followed by washing in ddH_2O and hematoxylin counterstain. The sections were dehydrated in graded alcohols, xylene, and finally mounted with Permount.

Results

Figure 2 shows NOE_{MTR} maps before (Fig. 2a) and after (Fig. 2b) Gd-DOTA administration, along with the calculated difference map (Fig. 2c), highlighting areas with the most pronounced contrast changes. The corresponding T1-weighted images (pre-contrast, post-Gd-DOTA) and the calculated difference maps are shown in Figs. 2d–f for comparison. The NOE_{MTR} difference map (Fig. 2c) reveals a clear reduction in NOE_{MTR} signal within both the tumor core and tumor periphery, while regions corresponding to the NABR exhibit no appreciable changes. Notably, no visible signal change was observed in the tumor periphery on the post-contrast T1-weighted image. However, overlaying the NOE_{MTR} difference map on the post-contrast T1-weighted image clearly delineates tumor boundaries beyond the regions enhanced on conventional post-contrast T1-weighted imaging. This superior delineation underscores the ability of NOE_{MTR} imaging to capture molecular-scale variations that may be missed by traditional contrast-enhanced MRI methods.

Quantitative analysis supports these visual observations. Following Gd-DOTA administration, the tumor core exhibited the largest percent decrease in NOE_{MTR} signal (−42.5%, p = 0.003), with an average drop from 29.2 ± 0.2 to 16.8 ± 1.3. The tumor periphery demonstrated a moderate reduction (−10.3%, p = 0.045) in NOE_{MTR} signal (from 38.3 ± 3.7 to 34.4 ± 5.0). In contrast, the NABR showed negligible change (+1.6%, p = 0.371), with values remaining stable (from 41.4 ± 1.7 to 42.1 ± 2.3). These findings emphasize the specificity of the NOE_{MTR} signal drop within tumor-associated tissue compartments.

In comparison, changes observed on T1-weighted images were more subtle and less spatially specific. The tumor core exhibited a 33.2% increase in T1 signal (from 12,956 ± 4,797 to 17,251 ± 6,361, p = 0.092), while the tumor periphery showed only a 3.8% increase (from

13,788 ± 2,922 to 14,310 ± 2,336, p = 0.478). NABR regions showed an 8.7% increase in T1 signal (from 11,618 ± 3,764 to 12,632 ± 1,905, p = 0.464), indicating statically not significant decrease in contrast differentiation between normal and tumor-adjacent tissues compared to NOE_{MTR} imaging. These results highlight the enhanced sensitivity and spatial specificity of NOE_{MTR} over conventional T1-weighted imaging in detecting subtle molecular alterations in and around the tumor.

To further validate these findings, histological analysis was performed. Figure 3 presents hematoxylin-eosin and ED1 stained tumor sections, revealing the spatial distribution of tumor core and tumor boundary. Zoomed-in regions from the tumor boundary, where post-Gd-DOTA NOE signal changes were observed, correspond to macrophage-rich regions containing infiltrative tumor cells, suggesting a biologically relevant transition zone between tumor tissue and adjacent normal brain (Fig. 4). Notably, the zoomed-in tumor region shows no signal enhancement on the post-contrast T1-weighted image at the tumor boundary (Fig. 4a).

Figure 5 illustrates a quantitative comparison of NOE_{MTR} contrast across distinct tissue compartments. The bar plot summarizes average NOE_{MTR} values within the tumor core, tumor periphery, and NABR on the contralateral side across all rats. The tumor core demonstrates the most pronounced NOE_{MTR} signal drop following Gd-DOTA administration, while the peritumoral region shows a moderate yet distinguishable decrease. In contrast, NOE_{MTR} values in the NABR remain largely unchanged, underscoring the specificity of the observed contrast alterations within tumor-associated regions.

Discussion

Our results demonstrate a marked improvement in tumor boundary visualization using NOE_{MTR} imaging, particularly in response to Gd-DOTA administration. ROI analysis revealed significant contrast differences across tumor regions, with a mean signal reduction of (~13%) in the tumor core and (~4%) in the tumor periphery, while the NABR remained largely unchanged (~1%). These findings highlight the sensitivity of NOE_{MTR} imaging to molecular interactions and altered macromolecular content in tumor regions.

NOE_{MTR} is more sensitive to depict the tumor boundary than postcontrast T_1-weighted imaging. As shown in the bar graph, although the change in T_1 signal intensity is not significant, it results

in a significant change in NOE_{MTR} contrast in both the tumor core and tumor boundary. While there is a slight, non-significant increase in post-contrast T_1 signal intensity in the NABR, it does not lead to a noticeable change in NOE_{MTR} contrast. This is likely because, in NABR, the T_1 signal change is primarily due the shortening of water proton T_1 in the circulating blood, and which does not have appreciable cross relaxation effects with the protons on lipid, or macromolecules in NABR.

In contrast, both the tumor core and boundary exhibit BBB leakage, allowing Gd-DOTA molecules to accumulate. This accumulation leads to T_1 shortening of water protons that are in direct contact with the membranous lipids and macromolecules of tumor cells. The significant cross-relaxation between these water protons and the aliphatic protons on lipids and macromolecules, which are exposed in the cancerous cells, contributes to the observed decrease in NOE-MTR contrast. The loss of ECM structure in tumor core/periphery leads to more mobile lipids and macromolecules that reduces the cross relaxation between water protons and aliphatic protons on the lipids and macromolecules, which manifests in the reduced NOE MTR effect. Since the disintegration of extracellular matrix structure is significantly higher in tumor core than that in the periphery, the reduction in NOE MTR is higher than that in the periphery. Notably, the NOE_{MTR} difference maps aligned with histological regions of tumor infiltration and immune activity, revealing a biological sensitivity that may be obscured in conventional MR imaging. The histological validation reveals strong spatial correspondence between NOE_{MTR} difference maps and the distribution of tumor cells and macrophages. This suggests that NOE_{MTR} imaging may also reflect aspects of the tumor immune response, adding potential value for characterizing tumor heterogeneity and guiding targeted therapies. Furthermore, NOE_{MTR}'s minimal variation in NABR signal post-contrast highlights its potential for reliable tumor-to-background discrimination in both pre- and post-Gd settings

A study using APT-weighted imaging showed no change in contrast from the tumor tissue following Gd administration[31]. This may be because the APT contrast in tumors arises from intracellular amide and amine protons associated with proteins and short peptide chains. Since tumor cells do not significantly uptake Gd-based contrast agents[32-33], there is no substantial reduction in the T1 relaxation time of intracellular water protons, which are in cross-relaxation with the exchangeable protons, and hence no change in the APT-weighted contrast.

PET/CT is one of the most widely used imaging modalities for characterizing tumors in clinical practice. A recent study highlighted that the widespread use of CT scans has raised significant

public health concerns due to the potential for radiation-induced cancers. Although children are more sensitive to radiation and face higher risk per scan, adults receive most CT exams, contributing to most of the projected future cancer cases, particularly lung, colon, leukemia, and bladder cancers[34]. If current usage and radiation dose practices continue, CT-related cancers could eventually comprise up to 5% of all new cancer diagnoses annually[34]. This risk may be further exacerbated by the increasing use of PET/CT scans, which combine two imaging modalities and deliver significantly higher radiation doses than standard CT alone[34-36], thereby amplifying cumulative exposure and the associated cancer risk. These findings underscore the urgent need to reduce unnecessary imaging and to optimize radiation doses across all modalities. In this context, MRI with non-ionizing radiation and improving capabilities for precise brain tumor delineation could serve as a safer alternative for certain clinical applications.

Since clinical imaging protocols for brain tumors already incorporate contrast-enhanced imaging, integrating NOE_{MTR} into the existing workflow offers a valuable opportunity to improve tumor characterization without requiring significant changes to current clinical practice. By leveraging the additional contrast provided by NOE_{MTR} particularly in regions of tumor infiltration that may appear normal on conventional imaging, this approach can improve the sensitivity and specificity of tumor boundary delineation. The ability to detect subtle changes in tissue microstructure and differentiate tumor from surrounding normal-appearing brain regions makes NOE_{MTR} a promising adjunct to standard contrast-enhanced MRI. Ultimately, incorporating NOE_{MTR} into routine clinical imaging could enable more accurate diagnosis, facilitate more precise treatment planning, and better monitoring of therapeutic response over time. While we have demonstrated the utility of this approach in characterizing a rat model of GBM, its underlying principles and advantages are broadly applicable to the clinical imaging of a wide range of solid tumors. As such, NOE_{MTR} holds significant potential for advancing oncologic imaging across multiple cancer types.

To further validate these findings, ongoing studies involving a larger cohort and concurrent IHC analyses aim to establish a stronger link between NOE_{MTR} contrast alterations and tumor biology. Given its improved differentiation of tumor regions, NOE_{MTR} imaging emerges as a promising alternative to existing conventional imaging methods for comprehensive tumor characterization. For proof-of-principle purposes, we employed a single slice using a two-dimensional imaging sequence. However, implementing a three-dimensional acquisition of NOE_{MTR} maps to enable complete brain tumor mapping would be relatively straightforward.

We further emphasize that High-resolution 3D-NOE_{MTR} maps will provide comprehensive images of the brain's anatomy, allowing for accurate delineation of tumor boundaries. These 3D-NOE_{MTR} maps can be transformed into 3D digital models, which can be 3D printed to produce physical replicas of the tumor core, tumor boundaries, and surrounding tissues (**supplementary figure 3**). Such models facilitate preoperative planning, allowing surgeons to rehearse procedures and anticipate challenges in a tangible format. Additionally, the detailed 3D map can be integrated into robotic surgery systems, allowing for real-time navigation and guidance during the procedure, improving accuracy, minimizing damage to healthy tissue, and enhancing patient outcomes.

Conclusion

Our findings suggest that NOE_{MTR} imaging, particularly in combination with Gd-DOTA administration, offers a significant advantage over conventional T_1-weighted MRI in delineating tumor boundaries with greater precision. By providing enhanced molecular contrast, NOE_{MTR} imaging allows for improved differentiation between the tumor core, peritumoral infiltration, and surrounding normal brain tissue. This capability has the potential to refine treatment planning, optimize surgical resection, and improve patient outcomes in oncology. Future studies will further explore the clinical translation of this technique, with the goal of integrating NOE_{MTR} imaging into routine neuro-oncological diagnostics and treatment assessment.

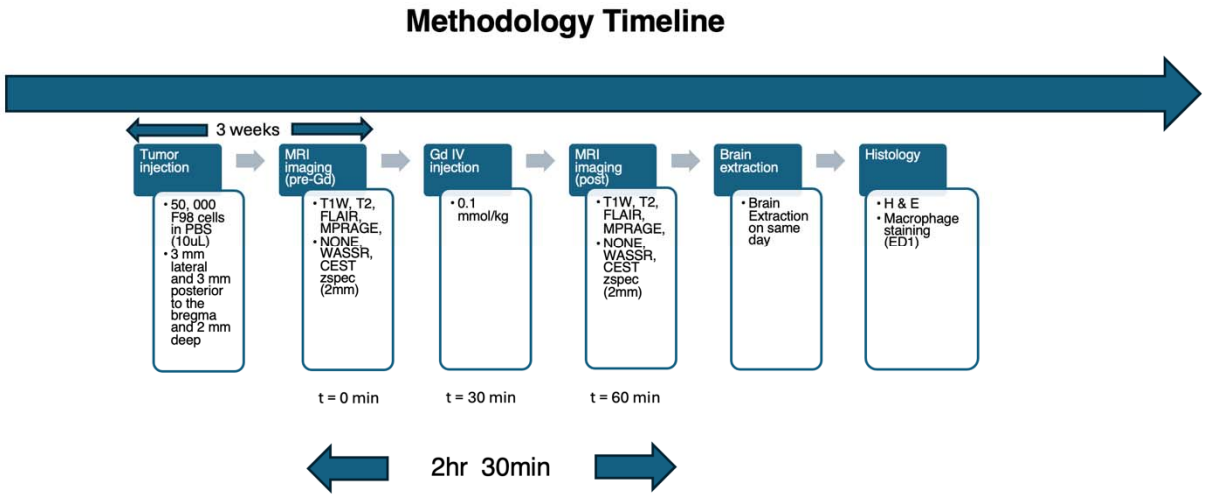

Figure 1: A timeline description of the methodology of this study. Rats were injected with the tumor cells (F98) and scanned three weeks later. pre- and post-Gd imaging was performed using the same MR sequences (T_1, T_2, CEST, NOE). The brains of these rats were extracted the same day for histological analysis (hematoxylin and ED1 staining).

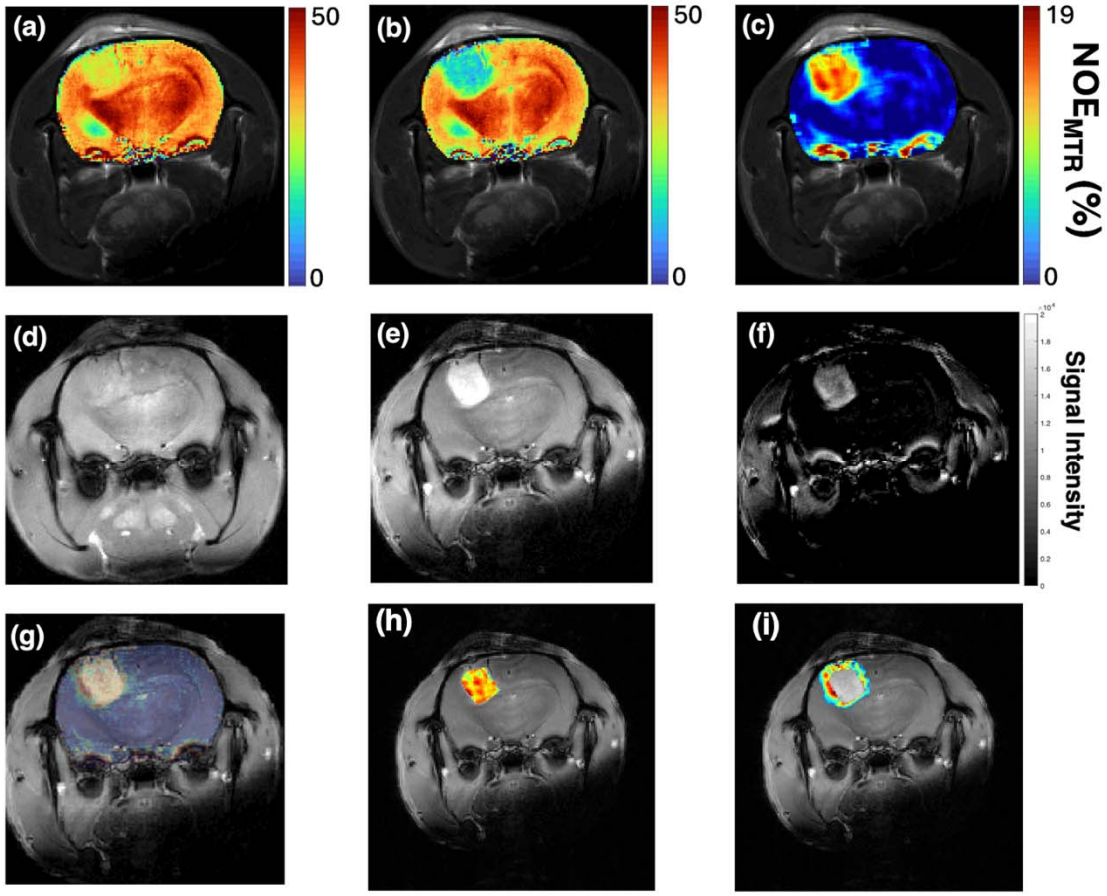

Figure 2: *In vivo* NOE_{MTR} maps from a brain tumor bearing rat brain before and after the infusion of gadoterate meglumine (Gd-DOTA). Image (a) displays the pre-infusion NOE_{MTR} map, while image (b) shows the post-infusion NOE_{MTR} map. Image (c) illustrates the subtraction of the post-infusion NOE_{MTR} map from the pre-infusion NOE_{MTR} map and image (d-f) displays the corresponding T_1-weighted pre-Gd, post-Gd, and difference map. The overlayed difference NOE_{MTR} map on the post-Gd T_1-weighted image (g), NOE difference map in the tumor core (h) and difference map outside the tumor core (i) highlights distinct tumor boundaries as compared to the post-Gd T_1-weighted image.

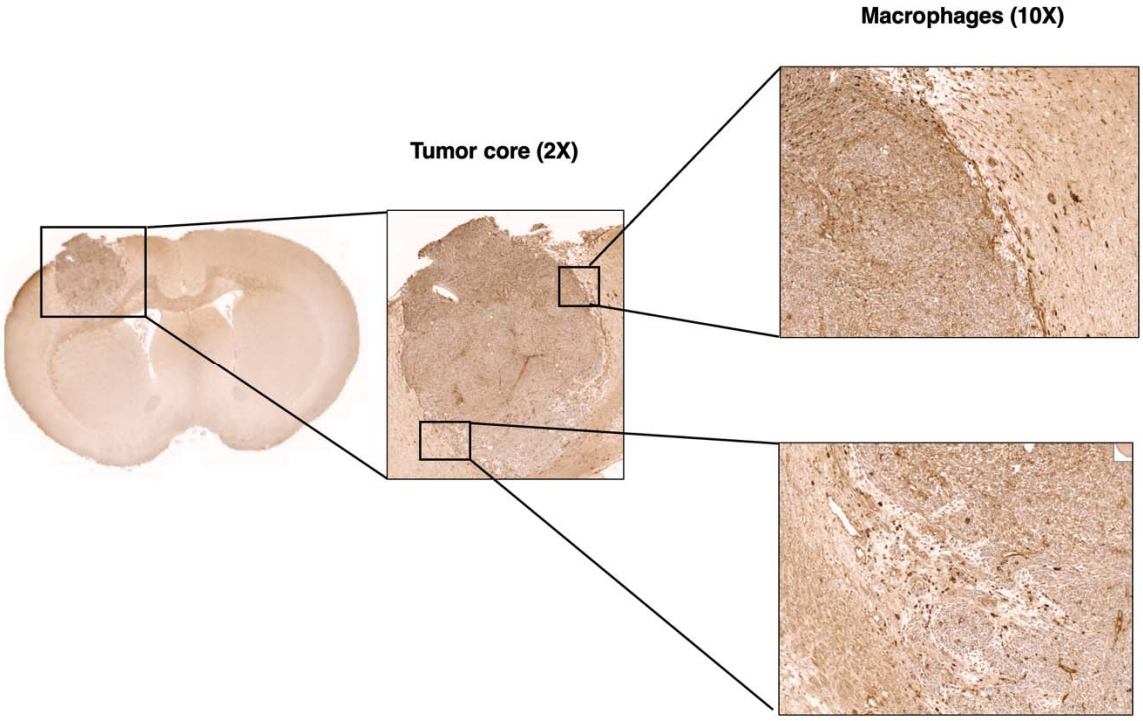

Figure 3: Immunohistochemical staining was performed using Hematoxylin and Anti-CD68 antibody [ED1] to visualize general tissue architecture and macrophage distribution, respectively. The hematoxylin-stained section shows the full brain slice corresponding to the tumor region from one representative rat, with zoomed-in views highlighting the tumor core, tumor boundary, and regions enriched with macrophages. ED1 staining confirms the presence of macrophages, particularly concentrated along the tumor periphery.

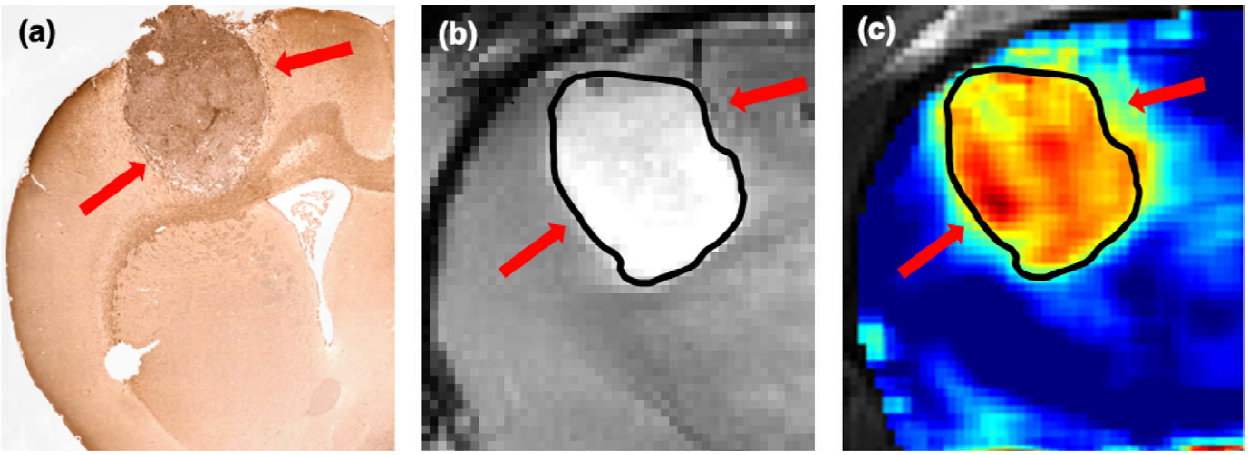

Figure 4: The zoomed-in tumor area shows clear uptake of Gd-DOTA contrast in the tumor on the post-contrast T_1-weighted image (a) but it does not demarcate the tumor boundary (red arrows). In contrast, the NOR_{MTR} difference map (b) highlights tumor regions extending beyond the signal observed on the post contrsat T_1-weighted image, which was further confirmed by the immunohistochemistry. The immunohistochemistry image clearly shows infilterated tumor cells and macrophage at the tumor periphery (red arrows).

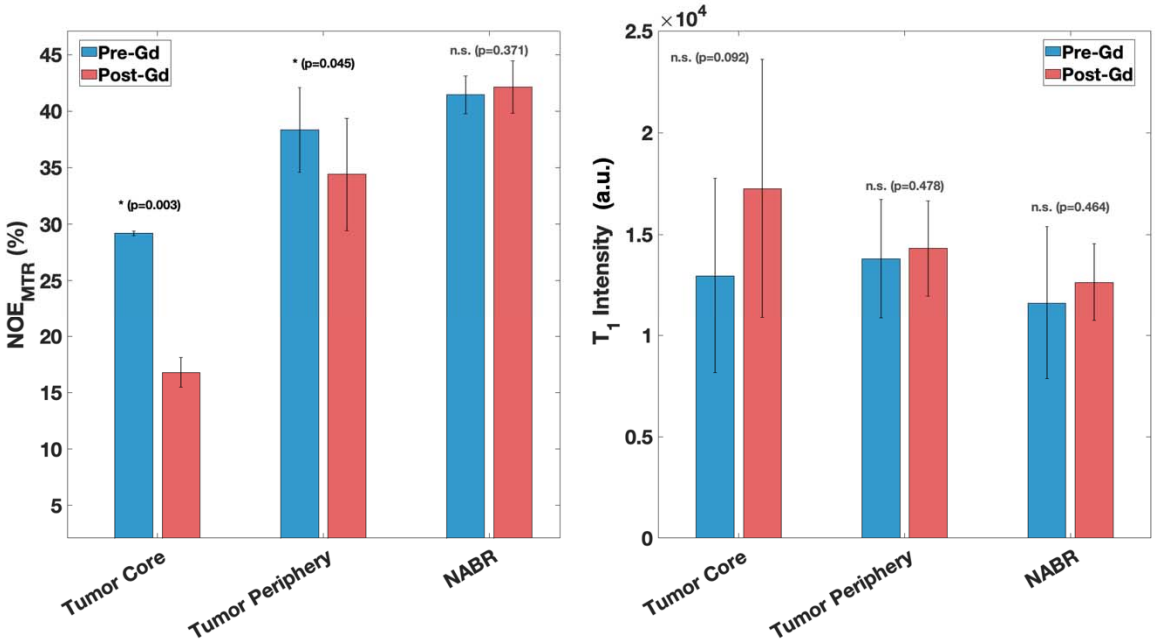

Figure 5: Bar plot representing average NOE_{MTR} percentages across regions of interest (ROIs) in the tumor core, tumor periphery, and contralateral normal-appearing brain region (NABR), measured pre- and post- Gd-DOTA infusion (n=5). A decrease in NOE contrast is observed in both tumor core and tumor periphery, while no appreciable change is observed in NABR.

Supplementary Information:

Supplementary figure 1 a presents another representative example of NOE_{MTR} maps from the rat brain tumor, demonstrating the clear differences pre- and post-Gd-DOTA administration. The corresponding NOE_{MTR} difference map provide better delineation of tumor boundary than post-Gd T_1-weighted image, further validating the technique's ability to capture contrast-enhanced tumor features. Supplementary figure 2 shows a comparison of averaged Z-spectra from regions of interest (ROIs) selected within the tumor core and NABR, both before and after Gd-DOTA administration. A substantial drop in NOE_{MTR} signal is observed in the tumor core following contrast infusion, consistent with the corresponding NOE_{MTR} maps shown in supplementary figure 1. This pronounced signal reduction suggests enhanced sensitivity of NOE_{MTR} imaging to molecular alterations induced by Gd-DOTA contrast agent, likely due to cross relaxation effects between water and macromolecules.

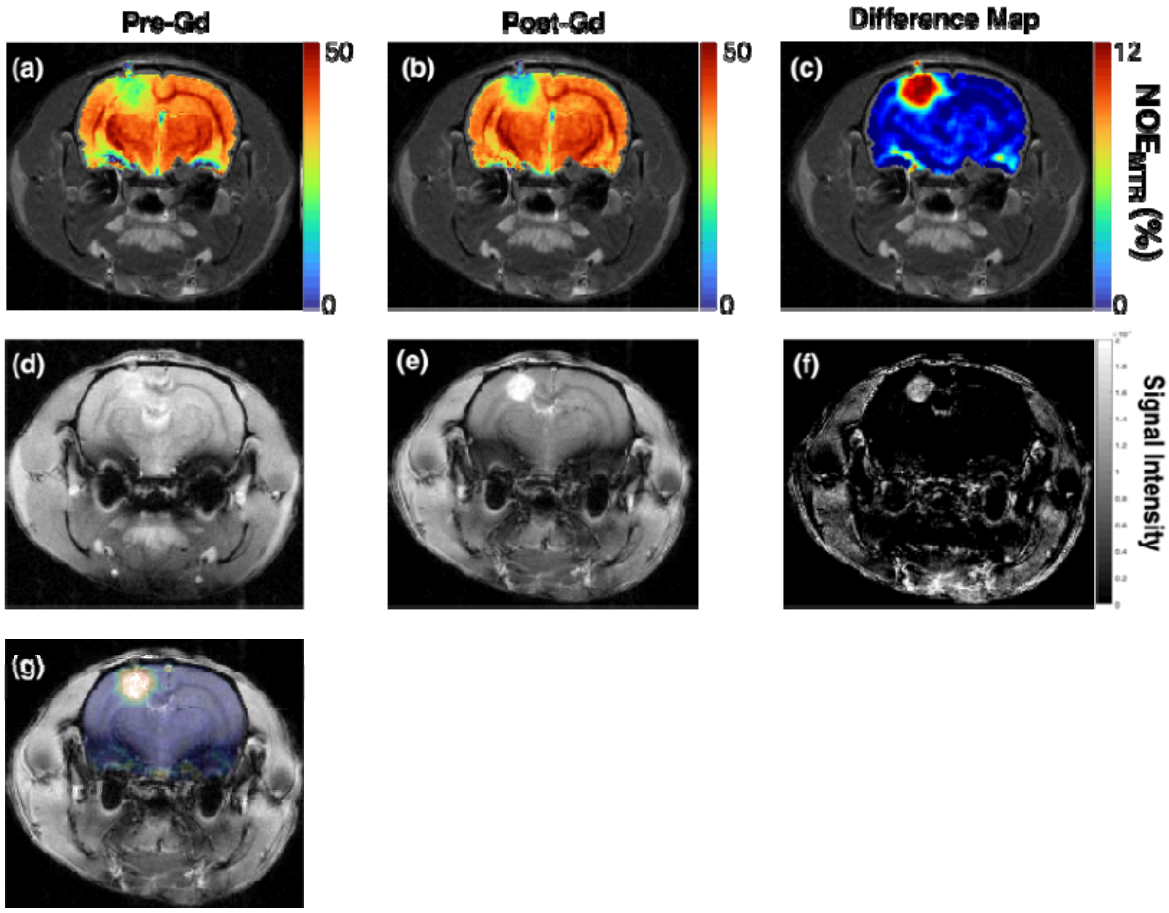

Supplementary figure 1: In vivo NOE_{MTR} maps from the brain tumor bearing rat brain in Figure 5 before and after the infusion of gadoterate meglumine (Gd-DOTA). Image (a) displays the pre-infusion NOE_{MTR} map, while image (b) shows the post-infusion NOE_{MTR} map. Image (c) illustrates the subtraction of the pre-infusion NOE_{MTR} map from the post-infusion NOE_{MTR} map and image (d-f) displays the corresponding T_1 weighted pre-Gd, post-Gd, and difference map. The subtracted NOE_{MTR} map (g) highlights distinct tumor boundaries as compared to the post-Gd T_1 weighted image.

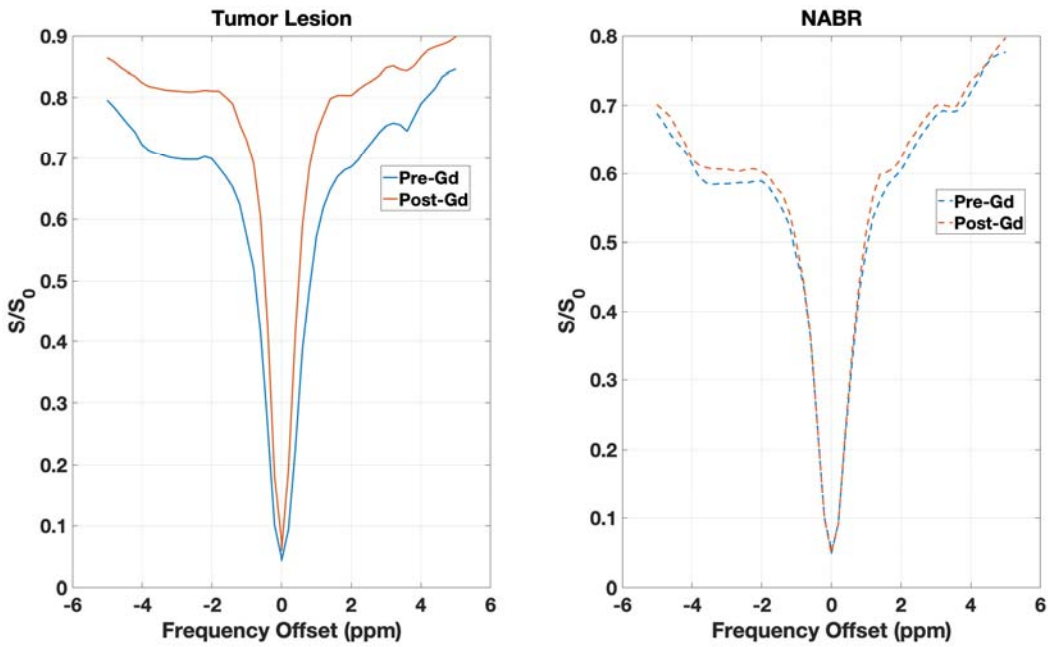

Supplementary figure 2: Z-spectra from the tumor core and the contralateral normal-appearing brain region (NABR) pre- and post-Gd treatment. Post-Gd Z-spectra demonstrate a clear decrease in NOE signal (-3.5ppm) from the tumor, while no appreciable change is observed in the NABR.

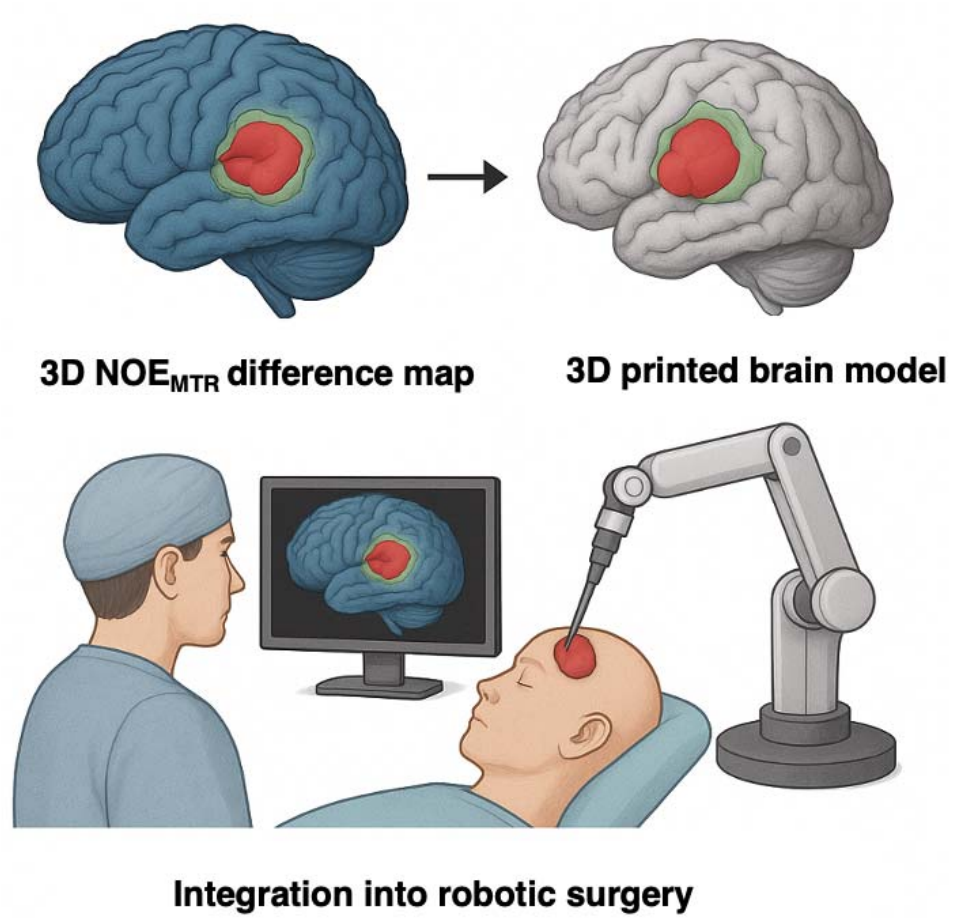

Supplementary Figure 3: This illustration demonstrates the clinical utility of high-resolution 3D-NOE$_{MTR}$ maps in brain tumor management. The top-left panel shows a digital 3D-NOE$_{MTR}$ brain map with clearly delineated tumor core (red) and surrounding boundary zones (green), enabling precise anatomical localization. The top-right panel depicts a corresponding 3D-printed brain model derived from these imaging data, representing a tangible replica of the tumor and adjacent structures for preoperative planning. The bottom panels illustrate the integration of the 3D-NOE$_{MTR}$ data into a robotic surgical system. This workflow enhances surgical precision, minimizes collateral tissue damage, and supports improved patient outcomes.

Acknowledgements

Research reported in this publication was supported by the National Institute on Aging of the National Institutes of Health under Award Numbers RF1AG087306, R01AG063869, and R01AG091760. Research reported in this publication was supported by the National Institute of Biomedical Imaging and Bioengineering of the National Institutes of Health under award Number P41EB029460.

References

1. Akakuru OU, Zhang Z, Iqbal MZ, Zhu C, Zhang Y, Wu A. Chemotherapeutic nanomaterials in tumor boundary delineation: Prospects for effective tumor treatment. *Acta Pharm Sin B*. 2022;12(6):2640-2657.
2. Matchett KB, Lynam-Lennon N, Watson RW, Brown JAL. Advances in Precision Medicine: Tailoring Individualized Therapies. Cancers (Basel). 2017;9(11):146.
3. Mirnezami R., Nicholson J., Darzi A. Preparing for precision medicine. N. Engl. J. Med. 2012; 366:489–491.
4. Ciardiello F., Arnold D., Casali P.G., Cervantes A., Douillard J.Y., Eggermont A., Eniu A., McGregor K., Peters S., Piccart M., et al. Delivering precision medicine in oncology today and in future-the promise and challenges of personalised cancer medicine: A position paper by the European Society for Medical Oncology (ESMO) Ann. Oncol. 2014; 25:1673–1678.
5. Ashley E.A. Towards precision medicine. Nat. Rev. Genet. 2016; 17:507–522.
6. Chen R., Snyder M. Promise of personalized omics to precision medicine. Wiley Interdiscip. Rev. Syst. Biol. Med. 2013; 5:73–82.
7. Molinaro AM, Hervey-Jumper S, Morshed RA, et al. Association of Maximal Extent of Resection of Contrast-Enhanced and Non-Contrast-Enhanced Tumor With Survival Within Molecular Subgroups of Patients With Newly Diagnosed Glioblastoma [published correction appears in JAMA Oncol. 2020 Mar 1;6(3):444.
8. Liu L, Liao C, Ge S, et al. Aggressive resection of non-contrast-enhanced tumor provides varying benefits to glioblastoma, IDH-wildtype patients based on different clinical characteristics. Cancer Lett. 2025;612:217471.
9. Jain R, et al. Pseudoprogression and pseudoresponse: Imaging challenges in the assessment of post-treatment glioma. Am J Neuroradiol. 2014;35(6):1160-1166.
10. Ellingson BM, et al. Pseudoprogression, radionecrosis, inflammation, or true tumor progression? Challenges associated with glioblastoma response assessment in an evolving therapeutic landscape. J Neurooncol. 2017;134(3):494-504.
11. Zong, Wei-Xing, and Craig B Thompson. “Necrotic death as a cell fate.” *Genes & development* vol. 20,1 (2006): 1-15.
12. Grivennikov, Sergei I et al. “Immunity, inflammation, and cancer.” *Cell* vol. 140,6 (2010): 883-99.
13. Yamaguchi F. The Border Zone of Tumor. Where is the Border? What is a Surgical Border for Patients?. World Neurosurg X. 2019; 2:100011.
14. Śledzińska-Bebyn P, Furtak J, Bebyn M, Serafin Z. Beyond conventional imaging: Advancements in MRI for glioma malignancy prediction and molecular profiling. Magn Reson Imaging. 2024;112:63-81.

15. Seker-Polat F, Pinarbasi Degirmenci N, Solaroglu I, Bagci-Onder T. Tumor Cell Infiltration into the Brain in Glioblastoma: From Mechanisms to Clinical Perspectives. Cancers (Basel). 2022;14(2):443.
16. Jones CK, Huang A, Xu J, et al. Nuclear Overhauser enhancement (NOE) imaging in the human brain at 7T. NeuroImage. 2013, 77, 114–124.
17. Zhou Y, Bie C, Zijl PCM, Yadav NN, et al. The relayed nuclear Overhauser effect in magnetization transfer and chemical exchange saturation transfer MRI. NMR in Biomedicine. 2022, e4778.
18. Zu Z, Lin EC, Louie EA, et al. Relayed nuclear Overhauser enhancement sensitivity to membrane Cho phospholipids. *Magn Reson Med*. 2020;84(4):1961-1976.
19. Benyard B, Nanga RPR, Wilson NE, et al. In vivo reproducibility of 3D relayed NOE in the healthy human brain at 7 T. *Magn Reson Med*. 2023;89(6):2295-2304
20. Swain A, Soni ND, Wilson N, et al. Early-stage mapping of macromolecular content in APP^{NL-F} mouse model of Alzheimer's disease using nuclear Overhauser effect MRI. *Front Aging Neurosci*. 2023; 15:1266859.
21. Paech D, Zaiss M, Meissner JE, et al. Nuclear overhauser enhancement mediated chemical exchange saturation transfer imaging at 7 Tesla in glioblastoma patients. PLoS One. 2014, 9(8):e104181.
22. Paech, D., Burth, S., Windschuh, J., et al. Nuclear Overhauser Enhancement imaging of glioblastoma at 7 Tesla: region specific correlation with apparent diffusion coefficient and histology. *PloS one*. 2015, *10*(3):e0121220.
23. Zaiss M, Windschuh J, Paech D, et al. Relaxation-compensated CEST- MRI of the human brain at 7 T: Unbiased insight into NOE and amide signal changes in human glioblastoma. Neuroimage. 2015, 112:180-188.
24. Windschuh J, Zaiss M, Meissner JE, et al. Correction of B1-inhomogeneities for relaxation-compensated CEST imaging at 7□T. NMR Biomed. 2015, 28(5):529-537.
25. Zaiss M, Zu Z, Xu J, et al. A combined analytical solution for chemical exchange saturation transfer and semi-solid magnetization transfer. NMR Biomed. 2015, 28(2):217-230.
26. Heo HY, Jones CK, Hua J, et al. Whole-brain amide proton transfer (APT) and nuclear overhauser enhancement (NOE) imaging in glioma patients using low-power steady- state pulsed chemical exchange saturation transfer (CEST) imaging at 7T. *J Magn Reson Imaging.* 2016, 44(1):41-50.
27. Mehrabian, H., Desmond, K. L., Soliman, H., et al. Differentiation between Radiation Necrosis and Tumor Progression Using Chemical Exchange Saturation Transfer. Clin Cancer Res. 2017, 23(14):3667-3675.
28. Zhang XY, Wang F, Jin T, et al. MR imaging of a novel NOE-mediated magnetization transfer with water in rat brain at 9.4T. Magn Reson Med. 2017, 78(2):588-597.
29. Wu, Y., Wood, T. C., Arzanforoosh, F., et al. 3D APT and NOE CEST-MRI of healthy volunteers and patients with non-enhancing glioma at 3 T. *Magma (New York, N.Y. 2022, 35*(1), 63–73

30. Mehrabi SF, Elmi S, Nylandsted J. Repurposing phenothiazines for cancer therapy: compromising membrane integrity in cancer cells. Front Oncol. 2023; 13:1320621.
31. Torrealdea, Francisco & Hearle, J & Evans, et al. APT-CEST post Gadolinium. Should it be avoided? Comparison of pre- & post- Gadolinium CEST on glioma at 3T. Intl. Soc. Mag. Reson. Med. 26 (2018).
32. Zhou Z, Lu ZR. Gadolinium-based contrast agents for magnetic resonance cancer imaging. Wiley Interdiscip Rev Nanomed Nanobiotechnol. 2013;5(1):1-18.
33. Aime S, Caravan P. Biodistribution of gadolinium-based contrast agents, including gadolinium deposition. J Magn Reson Imaging. 2009;30(6):1259-1267.
34. Smith-Bindman R, Chu PW, Azman Firdaus H, et al. Projected Lifetime Cancer Risks From Current Computed Tomography Imaging. JAMA Intern Med. Published online April 14, 2025.
35. Hosono M, Takenaka M, Monzen H, Tamura M, Kudo M, Nishimura Y. Cumulative radiation doses from recurrent PET-CT examinations. Br J Radiol. 2021;94(1126):20210388.
36. Indrakanti S, Li X, Rehani MM. Patients undergoing multiple 18F-FDG PET/CT exams: Assessment of frequency, dose and disease classification. Br J Radiol. 2022;95(1135):20211225.